spleen were removed with informed consent from an HIV-1–positive (diagnosed 5 years earlier) 32-year-old male bisexual on AZT with a CD4 T cell count of 2, hepatosplenomegaly, and MAC infection. Lymph nodes and spleen were heavily involved with MAC and were removed 6 months before death. No additional organisms were identified. Samples of the MAC-infected lymph nodes were paraffin embedded and unavailable for TEM.
11. J. M. Orenstein *et al.*, data not shown.
12. Y. Zhang, K. Nakata, M. Weiden, W. N. Rom, *J. Clin. Invest.* **95**, 2324 (1995); G. Poli *et al.*, *Proc. Natl. Acad. Sci. U.S.A.* **87**, 782 (1990).
13. S. M. Wahl and J. M. Orenstein, *J. Leukocyte Biol.*, in press.
14. A. S. Perelson, A. U. Neumann, M. Markowitz, J. M. Leonard, D. D. Ho, *Science* **271**, 1582 (1996).
15. C. M. Magro *et al.*, *Hum. Pathol.* **27**, 1066 (1996).
16. D. P. Chin *et al.*, *J. Infect. Dis.* **170**, 578 (1994); J. W. Pape, S. S. Jean, J. L. Ho, A. Hafner, W. D. Johnson, *Lancet* **342**, 268 (1993); E. R. Cooper, B. Damon, D. Reinke, A. Caliendo, S. I. Pelton, in *4th Conference on Retroviruses and Opportunistic Infections*, Washington, DC, 22 to 26 January 1997, p. 185; C. Whalen *et al.*, *AIDS (London)* **11**, 455 (1997).
17. M. Samson *et al.*, *Nature* **382**, 722 (1996); H. K. Deng *et al.*, *ibid.* **381**, 661 (1996); T. Dragic *et al.*, *ibid.*, p. 667; G. Alkhatib *et al.*, *Science* **272**, 1955 (1996); B. Doranz *et al.*, *Cell* **85**, 1149 (1996); H. Choe *et al.*, *ibid.*, p. 1135.
18. We thank C. Rehm, S. Hoover, C. Dye III, and S. Honig for technical assistance and K. Angelis for manuscript preparation. Supported in part by NIDR contract DE12585 (J.M.O.).

5 February 1997; accepted 5 May 1997

Crystal Structure of Human BPI and Two Bound Phospholipids at 2.4 Angstrom Resolution

Lesa J. Beamer, Stephen F. Carroll, David Eisenberg*

Bactericidal/permeability-increasing protein (BPI), a potent antimicrobial protein of 456 residues, binds to and neutralizes lipopolysaccharides from the outer membrane of Gram-negative bacteria. At a resolution of 2.4 angstroms, the crystal structure of human BPI shows a boomerang-shaped molecule formed by two similar domains. Two apolar pockets on the concave surface of the boomerang each bind a molecule of phosphatidylcholine, primarily by interacting with their acyl chains; this suggests that the pockets may also bind the acyl chains of lipopolysaccharide. As a model for the related plasma lipid transfer proteins, BPI illuminates a mechanism of lipid transfer for this protein family.

The outer membrane of Gram-negative bacteria contains the complex glycolipid lipopolysaccharide (LPS) (*1*). When present in the mammalian bloodstream, LPS elicits a powerful immune response that may include fever, hypotension, multiple organ failure, and, in severe cases, septic shock and death (*2*). In mammals, two related (45% sequence identity) LPS-binding proteins have been characterized that mediate the biological effects of LPS and participate in the innate immune response to bacterial infection: LPS-binding protein (LBP) and BPI. LBP is a plasma protein that enhances the inflammatory response to LPS (*3*), whereas BPI is found in lysosomal granules of polymorphonuclear neutrophils, is bactericidal, and neutralizes the toxic effects of LPS (*4*). Recombinant NH_2-terminal fragments of BPI retain biological activity (*5*), neutralize LPS in humans (*6*), and may have clinical utility (*4*).

BPI and LBP share functional and sequence similarity with two proteins responsible for lipid transport in the mammalian bloodstream (*7*). These plasma lipid transport proteins are involved in regulating the size, shape, and composition of lipoprotein particles such as high-density lipoproteins, and are not related to structurally characterized lipid-binding proteins such as the lipocalins (*8*). Here, we present the crystal structure of BPI and two bound phospholipids at 2.4 Å resolution. Our model provides the first structural information on the LPS-binding and lipid transport protein family and suggests a common mode of lipid binding for its members.

Purified, full-length, nonglycosylated, recombinant human BPI expressed in CHO cells was crystallized by hanging drop vapor diffusion at room temperature. The protein concentration was 8.5 mg/ml and the crystallization buffer contained 12% (w/v) polyethylene glycol (molecular weight 8000), 200 mM magnesium acetate, and 100 mM sodium cacodylate (pH 6.8). Two crystal forms with slightly different cell dimensions grow under the same conditions in space group C2, with one molecule per asymmetric unit. Form 1 crystals are reproducible and have cell dimensions of a = 185.0 Å, b = 37.2 Å, c = 84.3 Å, and β = 101.3°. Form 2 crystals appear rarely and have cell dimensions of a = 185.6 Å, b = 33.0 Å, c = 85.2 Å, and β = 101.6° (Tables 1 and 2).

BPI is a boomerang-shaped molecule with approximate dimensions of 135 by 35 by 35 Å (Fig. 1, A and B). It consists of two domains of similar size (NH_2- and COOH-terminals) that are connected by a proline-rich linker of 21 residues (positions 230 to 250). The two domains form three structural units; barrels are found at each end of the protein, and a central β sheet forms an interface between the barrels. The secondary structure and topology of the two domains are similar, giving the protein pseudo-twofold symmetry.

Each barrel (residues 10 to 193 and 260 to 421) contains three common structural elements: a short α helix, a five-stranded antiparallel β sheet, and a long helix (Fig. 2A), in that order. We call these elements helix A, sheet N, and helix B in the NH_2-terminal domain and helix A′, sheet C, and helix B′ in the COOH-terminal domain. Sheets N and C have a series of β bulges that change the direction of their strands and cause a pronounced curve in the sheets. In each domain, the long helix lies along the concave face of the sheet, with the helical axis at ~60° to the strands of the β

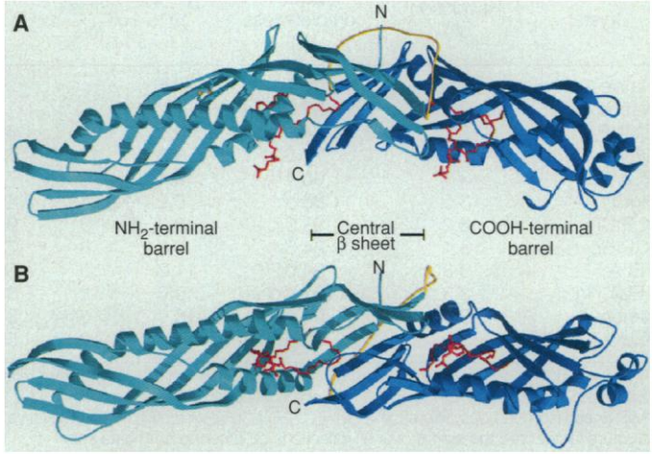

Fig. 1. (**A**) A ribbon diagram of residues 1 to 456 of BPI, illustrating its boomerang shape. The NH_2-terminal domain is shown in green, the COOH-terminal domain in blue, and the two phosphatidylcholine molecules in red. The linker is yellow, and the disulfide bond is shown as a ball-and-stick model. (**B**) View after rotating (A) 70° about the long axis of the molecule. Image produced with MOLSCRIPT (*30*) and RASTER3D (*31*).

L. J. Beamer and D. Eisenberg, UCLA-DOE Laboratory of Structural Biology and Molecular Medicine, Molecular Biology Institute, University of California, Los Angeles, CA 90095, USA.
S. F. Carroll, XOMA Corporation, 2910 Seventh Street, Berkeley, CA 94710, USA.
*To whom correspondence should be addressed.

sheet. A single disulfide bond between Cys^{135} and Cys^{175} anchors helix B to the final strand of sheet N. Situated between the NH_2- and COOH-terminal barrels is a twisted, seven-stranded antiparallel β sheet composed of four strands from the NH_2-terminal domain and three strands from the COOH-terminal domain. This central sheet forms an interface between the two domains and is thus reminiscent of several dimer interfaces stabilized by hydrogen bonds between strands of a β sheet (9).

The structural similarity of the two domains of BPI is shown by the superposition (*10*) in Fig. 2B; they are related by a rotation of 173° and have a root-mean-square deviation (rmsd) of 3.0 Å on the basis of superposition of 169 Cα pairs. The structure shared by these two domains does not resemble other protein folds; several structural alignment programs (*11*) failed to reveal a significant match to any known fold. Significant differences between the superimposed domains are found in two loop regions containing residues 45 and 96 in the NH_2-terminal domain and residues 280 and 348 in the COOH-terminal domain. These differences may be functionally important because the loops around residues 45 and 96 in the NH_2-terminal domain have been implicated in LPS-binding and bactericidal activity (see below). This structural similarity of the two domains was unexpected, not only because of their lack of significant sequence identity (<20%) but also because of their functional differences. The NH_2-terminal domain of BPI is cationic and retains the bactericidal, LPS-binding, and LPS-neutralization activities of the intact protein (*5*, *12*, *13*). The COOH-terminal domain is essentially neutral and shows limited LPS-neutralization activity (*14*). However, the structural similarity of the two domains may reflect a previously undetected functional similarity: Each domain contains a binding pocket for a phospholipid.

After the amino acid sequence had been traced in the electron density maps, two regions of extended electron density remained that could not be accounted for by protein atoms. This density, found in the interior of both domains, was present

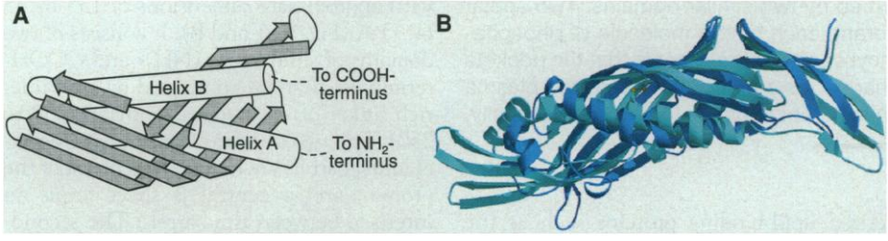

Fig. 2. (**A**) Schematic drawing of the BPI domain fold, shown in the same orientation as the NH_2-terminal domain in Fig. 1B. (**B**) Superposition of the NH_2- and COOH-terminal domains of BPI, showing the overall topological similarity. Residues 1 to 230 are green and 250 to 456 are blue. The NH_2-terminal domain is in the same orientation as in Fig. 1A.

Table 1. Structure determination. X-ray diffraction data were collected at room temperature with the R-AXIS IIC imaging plate area detector mounted on a Rigaku RU200 rotating anode x-ray generator. Data were processed with DENZO and SCALEPACK (*22*). For form 1 crystals, a native data set to 2.8 Å was collected from a single crystal, which was 92.4% complete overall [84.9% complete with an average $I/\sigma(I) = 2.3$ in the outermost resolution shell, where I is observed intensity and $\sigma(I)$ is its SD]. A native data set to 2.4 Å for form 2 was collected from two crystals and was 92.7% complete overall [94.6% complete with an average $I/\sigma(I) = 2.6$ in the outermost shell]. Because they could be reliably reproduced, form 1 crystals were used for all heavy atom soaks. The structure was solved by MIR with anomalous scattering. Heavy atom sites were identified by difference-Patterson and difference-Fourier maps. Phase refinement was performed with MLPHARE (*23*), producing a mean figure of merit (FOM) of 0.57. The MIR map (Fig. 3) was improved by density modification including solvent flattening, histogram matching, and phase extension using DM (*23*). After a partial model was obtained with FRODO (*24*), phase combination was performed with SIGMAA (*23*) (final FOM = 0.89). CMNP, chloro-Hg-nitrophenol; DMM, dimethyl mercury; PCMBS, parachloromercurybenzene sulfonate; TELA, triethyl lead acetate.

Crystal	Resolution (Å)	Data completeness (%)	R_{sym}* (%)	Sites (*N*)	R_{Cullis}†	Phasing power†	MID‡
Native 1	2.8	92.4	8.6				
Native 2	2.4	92.7	7.2				
CMNP	3.2	84.8	6.1	1	66.0	2.04	0.15
DMM	3.5	72.8	9.8	11	65.0	1.49	0.26
PCMBS	3.1	66.4	9.4	3	77.0	1.27	0.38
$HgCl_2$	3.0	86.5	6.9	1	49.0	2.13	0.18
K_2PtCl_4	3.2	93.3	8.2	3	90.0	0.68	0.13
K_2PtBr_6	3.1	94.8	5.8	3	73.0	0.88	0.14
TELA	3.3	94.0	11.3	2	86.0	0.80	0.15
TELA-$HgCl_2$	3.3	91.4	9.6	3	63.0	1.90	0.18
Xenon	3.4	98.2	18.9	5	87.0	0.69	0.18
$K_3UO_2F_5$	3.0	75.0	8.6	2	65.0	1.40	0.16

*$R_{sym} = 100(\Sigma_h|I_h - \langle I\rangle|)/(\Sigma_h I_h)$, where $\langle I\rangle$ is the mean intensity of all symmetry-related reflections I_h. †$R_{Cullis} = (\Sigma||F_{PH} \pm F_P| - F_{H(calc)}|)/(\Sigma|F_{PH} \pm F_P|)$ for centric reflections; phasing power = $[\Sigma F_{H(calc)}^2/(\Sigma F_{PH(obs)} - F_{PH(calc)})^2]^{1/2}$. ‡MID (mean isomorphous difference) = $\Sigma|F_{PH} - F_P|/\Sigma F_P$, where F_{PH} is the derivative structure factor, F_P is the native structure factor, and the sum is over all reflections common to both data sets.

Table 2. Model refinement and statistics for form 2 crystals. The model was refined at 2.8 Å through iterative cycles of simulated annealing with X-PLOR (*25*) and manual rebuilding; 10% of the data were set aside before refinement began for R_{free} (*26*) calculations. When the model had been refined to an R factor of 20.4% (R_{free} = 32.6%) with the 2.8 Å data, rigid-body minimization was performed against the 2.4 Å data set (R = 29.8% to 3.5 Å after minimization). Additional cycles of simulated annealing, positional refinement, correlated individual temperature factor refinement, and manual rebuilding reduced the R factor to 22.5% and R_{free} = 29.5% (no intensity cutoff). An overall anisotropic temperature factor and bulk solvent correction were used since R_{free} showed improvement. The model was confirmed by calculating simulated-annealing omit-maps for every part of the structure. The final model contains all 456 residues of the protein, 48 well-ordered waters, and two molecules of phosphatidylcholine. Regions of the backbone with poor electron density include residues 148, 232 to 236, 258 to 260, and parts of the loop between residues 281 and 311. Side chains with poorly defined density were truncated to alanine. The model was examined with the programs PROCHECK (*27*), VERIFY (*28*), and ERRAT (*29*).

Data	
Resolution (Å)	2.4
Unique reflections (*N*)	18,808
Completeness (%)	92.7
Atoms in model	
Protein (non-hydrogen)	3531
Phosphatidylcholine	102
Water	48
Refinement parameters	
Resolution range (Å)	50.0 to 2.4
R factor* (%)	22.5
R_{free} (%)	29.5
Average atomic B factors	
Protein	44.5
Lipid N, C	56.9, 59.0†
Waters	53.1
Deviation from ideality (rmsd)	
Bonds (Å)	0.007
Angles (°)	1.4
Dihedrals (°)	26.0
Impropers (°)	1.2

*$R = 100(\Sigma|F_{obs} - F_{calc}|)/(\Sigma F_{obs})$, where F_{obs} and F_{calc} are the observed and calculated structure factors, respectively. †B factors for the lipids bound in the NH_2- and COOH-terminal domains.

in the multiple isomorphous replacement (MIR) maps (Fig. 3) at an intensity similar to that of the protein density, and it became the predominant feature in $F_{obs} - F_{calc}$ maps after sequence fitting (both form 1 and form 2 crystals). Electrospray mass spectrometry of the sample used for crystallization revealed two molecules, with relative molecular masses of 522 and 787, in approximately equal amounts. Tandem mass spectrometric analysis was consistent with the two species being phosphoglycerides containing a phosphatidylcholine head group and either one or two 18-carbon acyl chains with one double bond. Phosphatidylcholine (Fig. 4A) is abundant in eukaryotic cells and is presumably bound by BPI in the cells from which the protein is isolated.

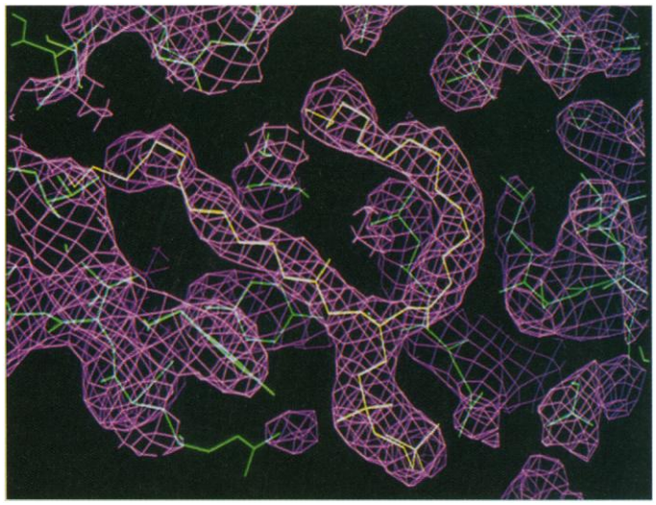

Fig. 3. Electron density (purple) of the final 2.8 Å MIR map contoured at 1.0σ and superimposed on the refined model. The area shown is in the lipid-binding pocket of the NH_2-terminal domain of BPI. The phosphatidylcholine is yellow and the surrounding protein atoms are green.

The two lipids are bound in extensive apolar pockets on the concave surface of the boomerang, situated between the NH_2- and COOH-terminal barrels and the central β sheet. In the NH_2-terminal domain, the entrance to the pocket is formed by helices A and B. The back and sides are formed by sheet N and the central sheet. The two acyl chains insert ~15 Å into the interior of the protein and are surrounded

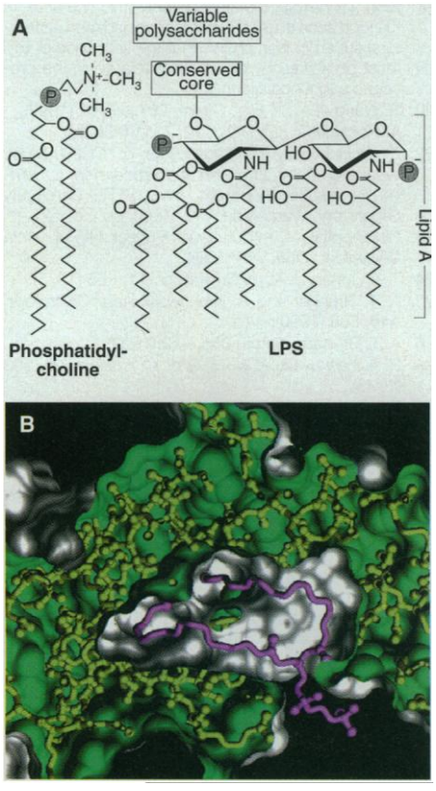

Fig. 4. (**A**) Covalent structure of phosphatidylcholine and the lipid A region of LPS from *E. coli* and *S. typhimurium*. Phosphate groups are indicated by P. Adapted, with changes, from (*1*). (**B**) Slice through the interior of BPI showing the lipid-binding pocket in the NH_2-terminal domain. The solvent-accessible surface of the protein was calculated without lipid present and is shown in white, the interior of the protein is green, and the phosphatidylcholine is purple. Protein residues are shown as ball-and-stick in yellow. Image produced with MSP (*15*).

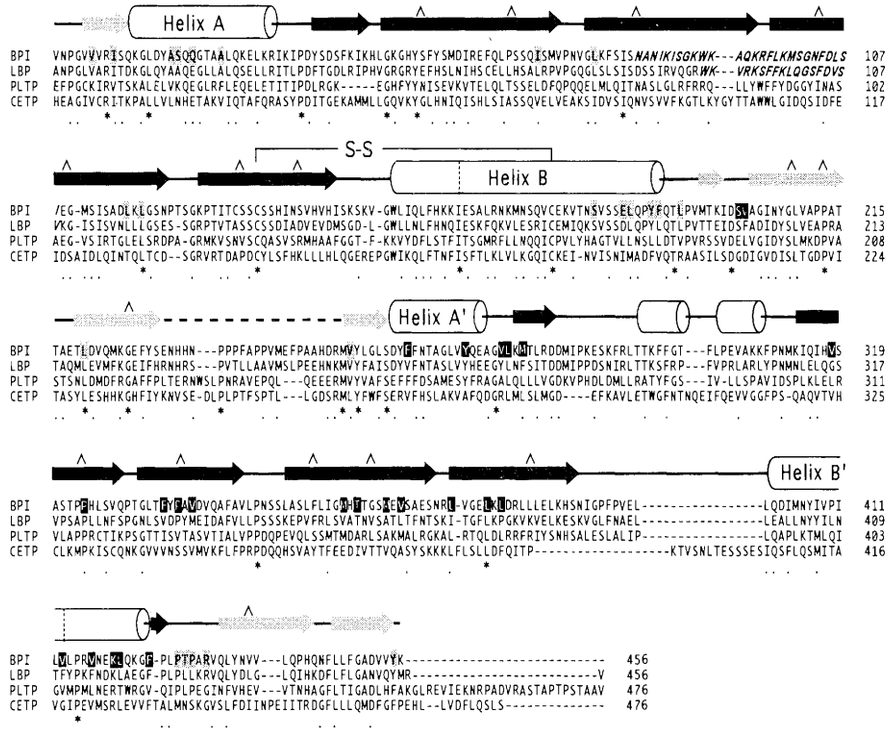

Fig. 5. Amino acid sequences of human BPI, LBP, PLTP, and CETP. The alignment was performed with CLUSTAL (*32*) using all 11 known protein sequences from mammals (*3, 33*), but only the four human sequences are shown. Residues that are completely conserved in all proteins are indicated by an asterisk below the sequence; those that are highly conserved are indicated by a dot. The secondary structure of BPI is indicated above the sequences. The β strands are indicated by arrows; strands that make up the central β sheet are shown with gray arrows. Because of the β bulges and pronounced twisting, some of the β strands have one or more residues that do not show classical H-bonding patterns or φψ angles; these breaks are indicated by ^ above the strands. The α helices are shown as cylinders, and one-residue breaks in helices B and B′ are indicated with a vertical dashed line. The horizontal dashed line indicates the linker region. Peptides from BPI and LBP with the highest LPS-binding activity (*18, 34*) are in bold italics. The disulfide bond is indicated by S-S. Residues with atoms within 4 Å of the NH_2-terminal lipid are shaded; residues within 4 Å of the COOH-terminal lipid are shown in reverse type. Abbreviations for the amino acid residues are as follows: A, Ala; C, Cys; D, Asp; E, Glu; F, Phe; G, Gly; H, His; I, Ile; K, Lys; L, Leu; M, Met; N, Asn; P, Pro; Q, Gln; R, Arg; S, Ser; T, Thr; V, Val; W, Trp; and Y, Tyr.

by apolar side chains (Fig. 4B). The head group lies at the entrance of the pocket and is exposed to solvent. The pocket in the COOH-terminal domain, which has a slightly larger opening, is formed by the analogous secondary structures. Both basic and acidic side chains found near the entrances of the pockets are available for electrostatic interactions with the zwitterionic head group. When the lipids are removed from the model, the pocket in the NH_2-terminal domain has a solvent-accessible surface area (*15*) of 557 Å^2 and the pocket in the COOH-terminal domain has an area of 413 Å^2, for a total of 970 Å^2. The intensity of the electron density for the two acyl chains in both pockets is similar and does not indicate whether the single acyl chain species is found predominantly in either pocket.

The discovery of bound phospholipid in the BPI structure suggests a possible site of interaction between BPI and LPS. Phosphatidylcholine and LPS share some structural similarity, including negatively charged phosphate groups and, most notably, acyl chains (Fig. 4A). Because BPI's function is to bind a lipid (LPS) and because a lipid is bound in pockets of BPI, it seems reasonable that acyl chains of LPS bind in the apolar pockets. The following observations support this hypothesis: (i) The acyl chains of lipid A are known to be essential for binding by BPI (*16*); (ii) the binding pockets of BPI are reminiscent of cavities in other lipid-binding proteins (*8*); and (iii) BPI has significant sequence similarity to two lipid transfer proteins (see below).

Our proposed site of interaction between BPI and the acyl chains of LPS differs from that suggested by previous work focusing on the NH_2-terminal domain. Fragments containing the NH_2-terminal domain of BPI have been identified with equivalent or greater bactericidal and LPS-binding activities relative to the full-length protein (*5*, *13*). The activity of one NH_2-terminal fragment was reduced when residues past position 12 or between positions 169 and 199 were deleted (*17*). The structure shows that these deletions affect elements of the barrel (at the beginning of helix A and from the middle to the end of helix B) and could alter its structure. Although the barrel seems to be the minimal structural unit with full activity, three smaller regions of this domain retain LPS-binding, LPS-neutralization, and bactericidal activity (*18*): residues 17 to 45 (most of helix A and the first β strand of sheet N), residues 82 to 108 [a β hairpin (*19*) between strands 3 and 4 of sheet N], and residues 142 to 169 (a segment preceding and including part of helix B). These three regions include 18 basic residues (and only four acidic residues) and form a positively charged tip on the NH_2-terminal domain (Fig. 1, left) that may make favorable electrostatic interactions with negatively charged groups of LPS. Further studies are necessary to determine the relative importance of the apolar pockets and the positively charged NH_2-terminal tip to BPI's LPS-binding and bactericidal activities.

BPI is the first member of the mammalian LPS-binding and lipid transfer family to have its three-dimensional structure determined. BPI and LBP are related to two lipid transfer proteins, cholesteryl ester transfer protein (CETP) and phospholipid transfer protein (PLTP) (*7*). Alignment of the amino acid sequences of human BPI, LBP, CETP, and PLTP with BPI's secondary structure (Fig. 5) shows that structurally important residues are conserved in the four proteins. The two cysteines that form the single disulfide bond and are critical to the function of BPI (*5*) are completely conserved. Also, the pattern of hydrophobic and hydrophilic residues in the β strands indicates that the β bulges responsible for the extensive sheet twisting are preserved. The conserved sequences strongly suggest that members of the LPS-binding and lipid transfer family share BPI's two-domain structure and that the two domains are similar in topology.

It is likely that the lipid transfer proteins also share the apolar binding pockets found in BPI. Striking parallels are found between our BPI-phosphatidylcholine structure and previous work showing that CETP copurifies with an equimolar amount of phosphatidylcholine (*7*) and has two distinct binding sites (*20*)—one for neutral lipids and another for phospholipids. The known ligands of CETP and PLTP (cholesteryl esters, triglycerides, retinyl esters, and phospholipids) all contain at least one acyl chain that could bind in apolar pockets similar to those in BPI, which suggests a common mode of ligand binding in this family. Sequestration of these hydrophobic chains in interior pockets may be critical to the function of the lipid transfer proteins: transfer of apolar ligands in an aqueous environment. Thus, the structure of BPI illuminates the action of the plasma lipid transfer proteins and may lead to a better understanding of how BPI and LBP interact with LPS.

REFERENCES AND NOTES

1. C. R. H. Raetz, *Annu. Rev. Biochem.* **59**, 129 (1990).
2. D. Heumann and M. P. Glauser, *Sci. Am. Sci. Med.* (November–December 1994), p. 28.
3. R. R. Schumann *et al.*, *Science* **249**, 1429 (1990).
4. P. Elsbach and J. Weiss, *Infect. Agents Dis.* **4**, 102 (1995).
5. A. H. Horwitz *et al.*, *Protein Expr. Purif.* **8**, 28 (1996).
6. M. A. N. von der Mohlen *et al.*, *J. Infect. Dis.* **172**, 144 (1995).
7. A. Tall, *Annu. Rev. Biochem.* **64**, 235 (1995).
8. L. Banaszak *et al.*, *Adv. Protein Chem.* **45**, 89 (1994).
9. M. Leeson *et al.*, *Structure* **4**, 253 (1996); D. Ohlendorf *et al.*, *J. Mol. Biol.* **169**, 757 (1983); G. N. Reeke *et al.*, *J. Biol. Chem.* **250**, 1525 (1975).
10. G. H. Cohen, *J. Mol. Biol.* **190**, 593 (1986).
11. N. N. Alexandrov and D. Fischer, *Proteins Struct. Funct. Genet.* **25**, 354 (1996); D. Fischer, C. J. Tsai, R. Nussinov, *Protein Eng.* **8**, 981 (1995); L. Holm and C. Sander, *Nucleic Acids Res.* **25**, 341 (1996).
12. C. E. Ooi *et al.*, *J. Biol. Chem.* **262**, 14891 (1987).
13. C. E. Ooi *et al.*, *J. Exp. Med.* **174**, 649 (1991).
14. S. L. Abrahamson *et al.*, *J. Biol. Chem.* **272**, 2149 (1997).
15. M. L. Connolly, *Science* **221**, 709 (1983); *J. Am. Chem. Soc.* **107**, 1118 (1985).
16. H. Gazzano-Santoro *et al.*, *Infect. Immun.* **63**, 2201 (1995).
17. C. Capodici and J. Weiss, *J. Immunol.* **156**, 4789 (1996).
18. R. G. Little *et al.*, *J. Biol. Chem.* **269**, 1865 (1994).
19. Residues 82 to 106 of BPI show limited sequence similarity with residues 32 to 51 of the *limulus* anti-LPS factor (LALF) and have been predicted to form an amphipathic β hairpin similar to that seen in the LALF structure (*21*). Although this region of BPI does form a β hairpin, the strict amphipathic character of the loop seen in LALF is not maintained, and a structural superposition shows that the sequence of BPI must be shifted by one residue relative to the proposed sequence alignment.
20. S. Wang *et al.*, *J. Biol. Chem.* **267**, 17487 (1992).
21. A. Hoess *et al.*, *EMBO J.* **12**, 3351 (1993).
22. Z. Otwinowski, in *Proceedings of CCP4 Study Weekend: Data Collection and Processing*, L. Sawyer, N. Isaacs, S. Baileys, Eds. (SERC Daresbury Laboratory, Warrington, UK, 1993), pp. 56–62.
23. Collaborative Computational Project No. 4, *Acta Crystallogr.* **D50**, 760 (1994).
24. T. A. Jones, *J. Appl. Crystallogr.* **11**, 268 (1978).
25. A. T. Brünger and A. Krukowski, *Acta Crystallogr.* **A46**, 585 (1990).
26. A. T. Brünger, *Nature* **355**, 472 (1992).
27. R. A. Laskowski *et al.*, *J. Appl. Crystallogr.* **26**, 283 (1993).
28. R. Lüthy *et al.*, *Nature* **356**, 83 (1992).
29. C. Colovos and T. Yeates, *Protein Sci.* **2**, 1511 (1993).
30. P. Kraulis, *J. Appl. Crystallogr.* **24**, 946 (1991).
31. E. A. Merritt and M. E. P. Murphy, *Acta Crystallogr.* **D50**, 869 (1994); D. J. Bacon and W. F. Anderson, *J. Mol. Graphics* **6**, 219 (1988).
32. D. G. Higgins and P. M. Sharp, *Gene* **73**, 237 (1989).
33. D. Drayna *et al.*, *Nature* **327**, 632 (1987); R. Day *et al.*, *J. Biol. Chem.* **269**, 9388 (1994); S. R. Leong and T. Camerato, *Nucleic Acids Res.* **18**, 3052 (1990); M. Nagashima *et al.*, *J. Lipid Res.* **29**, 1643 (1988); M. E. Pape *et al.*, *Arteriosclerosis* **11**, 1759 (1991); G. Su *et al.*, *J. Immunol.* **153**, 743 (1994); P. W. Gray *et al.*, *J. Biol. Chem.* **264**, 9505 (1989); J. J. Albers *et al.*, *Biochim. Biophys. Acta* **1258**, 27 (1995); X.-c. Jiang *et al.*, *Biochemistry* **34**, 7258 (1995); L. B. Agellon *et al.*, *ibid.* **29**, 1372 (1990); X.-c. Jiang *et al.*, *J. Biol. Chem.* **266**, 4631 (1991).
34. A. H. Taylor *et al.*, *J. Biol. Chem.* **270**, 17934 (1995).

35. We thank S. Abrahamson, E. Bautista, P. Gavit, A. Horwitz, G. Theofan, and J. Weickmann for protein preparation, T. Le for crystallization, R. Liddington for coordinates of LALF, M. Stowell for use of the xenon pressure apparatus, K. Faull for mass spectrometry, and M. Bennett and M. Weiss for discussions. Supported by NIH grant GM31299 and by the U.S. Department of Energy. Coordinates have been deposited in the Brookhaven Protein Data Bank (ID code 1bp1).

21 November 1996; accepted 18 April 1997